Check for updates

Enhancing N_2 Fixation Activity by Converting Ti_3C_2 MXenes Nanosheets to Nanoribbons

Hua Wei[+],[a, c] Qian Jiang[+],[b] Claudio Ampelli,[a] Shiming Chen,[b] Siglinda Perathoner,[a] Yuefeng Liu,*[b] and Gabriele Centi*[a]

Metal carbides M_2C (MXenes) with two-dimensional (2D) structure have been indicated as promising materials for N_2 fixation, with the activity being related to edge planes. Here, it is instead demonstrated that the transformation from a 2D- (nanosheets) to a 3D-type nanostructure (nanoribbons) leads to a significant enhancement of the N_2 fixation activity due to the formation of exposed Ti–OH sites. A linear relationship is observed between ammonia formation rate and amount of oxygen on the surface of Ti_3C_2 MXene.

MXenes are metal carbide or nitride materials with a two-dimensional (2D) structure, which attracted a large interest recently for a broad range of applications such as materials for energy and environmental applications,[1–4] and catalysis.[5–7] In the latter area, several papers deal on N_2 fixation (NRR),[8–18] a topic of current large interest to directly produce ammonia from nitrogen.[19] MXene presents the unusual electronic property of the 2D structure and also the unique property of transition metal carbides, such as metallic conductivity, and the hydrophilic nature of their hydroxyl or oxygen terminated surfaces. For these properties there is a large interest on the use of MXenes as novel NRR electrocatalysts, as emerges also from the state-of-the-art comparison of NRR electrocatalysts (see Table S2 in the Supporting Information). They have properties well comparable with those of the best reported NRR electrocatalysts, with the advantage of a flexible way to tune further their properties, and thus a large potential for further improvement.

Most of studies on MXenes as NRR materials indicated the need to have a 2D nanostructure, with the activity in N_2 fixation attributed generally to edge sites of the nanosheets. Luo et al.,[16] for example, indicate the middle Ti at the edge sites as the active sites for NRR. The mechanism proposed involved hydrogenation of undissociated N_2 molecules. Gouveia et al.[6] considered instead that N_2 dissociation occurs easily on the MXene (0001) surface. The top site above the metal ions on the surface of MXene nanosheets was also indicated by Wang et al.[9a] as the sites for end-on adsorption of N_2 which is then hydrogenated, rather than dissociated. Johnson et al.[15] indicated that edge sites of MXene are involved in NRR reaction and that F functional groups enhance the NRR performance in comparison to O functional groups. Xia et al.,[11] on the contrary, indicated that exposed Ti sites in Ti_3C_2OH facilitate the electron transfer and promote the adsorption and activation of dinitrogen. Guo et al.[12] suggested that OH terminal groups of MXene are inactive, indicating thus that a modification of the surface chemical states by introducing Fe heteroatoms is necessary to increase the activity.

Most of the studies based their conclusions mainly on theoretical modelling. However, notwithstanding the discordances in the nature of the active MXene materials for NRR reaction, a common agreement is that a 2D configuration is needed.

2D-type materials are an area of intense research interest for a number of applications in the field of materials for energy, including catalysis.[20] On the other hand, it is possible to assemble and master 2D materials to form other type of 3D-like nanomaterials.[21] MXenes nanosheets can be subjected to a transformation from a 2D to a 3D-like nanostructures.[22] This will allow to clarify the relationship between performances and type of nanostructure. In the specific case of NRR, this method of manipulating nanostructures allows to understand the role and relevance of the presence of a 2D nanostructure on edge or planar bases, by comparing the behaviour of very analogous materials but with different nanoshapes.

We have thus investigated how the conversion of Ti_3C_2 nanosheets to 3D-like nanoribbons influence the properties and NRR reactivity to obtain insights about the role of the nanostructure in this reaction providing therefore elements for theoretical modelling to overcome the present discordances on the nature of the active materials and thus allow their better design.

[a] Dr. H. Wei,[+] Prof. C. Ampelli, Prof. S. Perathoner, Prof. G. Centi
Dept.s ChimBioFarAm and MIFT
Università degli Studi di Messina
D'Alcontres 31 V.le F. Stagno
98166 Messina (Italy)
E-mail: centi@unime.it
[b] Dr. Q. Jiang,[+] Dr. S. Chen, Prof. Y. Liu
Dalian National Laboratory for Clean Energy
Dalian Institute of Chemical Physics
Chinese Academy of Sciences
457 Zhongshan Road, Dalian 116023 (P. R. China)
E-mail: yuefeng.liu@dicp.ac.cn
[c] Dr. H. Wei[+]
Univ.Lyon, Universite Claude Bernard Lyon 1
CNRS, IRCELYON – UMR5256
2 Av. Albert Einstein
69626 Villeurbanne (France)
[+] These authors contributed equally to this work.

Supporting inforfmation for this article is available on the WWW under https://doi.org/10.1002/cssc.202001719

This publication is part of a Special Collection highlighting "The Latest Research from our Board Members". Please visit the Special Collection at https://bit.ly/cscBoardMembers.

© 2020 Wiley-VCH GmbH

Ti_3C_2 MXene nanosheets (MNSs) were prepared by HF etching (in 40% HF solution for 72 h) of Ti_3AlC_2 starting precursor, followed by centrifugation, washing and drying at 60 °C. The obtained MNSs are then treated in 6 M KOH for 72 h (sealed container under Ar atmosphere), followed by steps as above. Ti_3C_2 MXene nanoribbons (MNRs) are obtained in this way. The method of preparation is analogous to that used by Lian et al.[23] MNSs and MNRs were dispersed in ethanol containing 10% Nafion (ultrasonic mixing for 90 min), obtaining a homogenous ink which is then deposited by spray drying onto a gas-diffusion layer (GDL). The GDL with the deposited electrocatalyst is then hot pressed to a Nafion membrane. The electrocatalyst is located at the interface between the Nafion membrane and the GDL. The loading of the electrocatalyst resulted 0.2 mg cm^{-2}.

The electrodes were tested in an electrocatalytic flow reactor, where the hemi-cell for NRR reaction operates without a liquid electrolyte. This type of electrocatalytic reactor is different from the conventional electrocatalytic reactors operating with the electrodes immersed in a liquid electrolyte. The reason is to avoid issues related to low N_2 solubility in the electrolyte, and to allow an easier recovery of the ammonia produced. In fact, NH_3 is recovered directly from the gas outlet of the flow reactor. Details on the preparation of the electrodes, although by using different type of electrocatalysts, and on the characteristics of the electrocatalytic reactor were reported earlier.[24–26] Figure S1 in the Supporting Information and related description reports also details about the flow electrocatalytic reactor, the experimental procedure of testing, the determination of ammonia and other possible products, and the series of control experiments made to verify that ammonia derives effectively from the electrocatalytic reduction of N_2.

The scanning electron microscopy (SEM) images (Figure 1a) for $Ti_3C_2T_x$ (where T=F, OH) after the HF etching, show a MXene loosely layered 2D structure, indicating the successful exfoliation of Al from the MAX phase (Ti_3C_2Al). The transparency of the nanosheet presented in Figure 1b suggests that the likely presence of single layer sheet.[27] It presents a monocrystal as shown by diffraction pots of the selected area electron diffraction (SAED) reported in the inset of Figure 1b. The HRTEM image (Figure 1c) shows the interlayer spacing of 1.00 nm corresponding to the (002) plane,[28] which is consistent with the value measured by XRD and with results obtained by Ghidiu et al.[29] After Ti_3C_2 nanosheets treatment by KOH, nanoribbons could be well evidenced (Figure 1d). The nanoribbons have a diameter around 16 nm, in agreement also with HRTEM images (Figure 1e and f).

The conversion of Ti_3AlC_2 (MAX phase) to Ti_3C_2 MNSs and MNRs is confirmed by X-ray diffraction (XRD) (Figure 2a). Compared with the pattern of Ti_3AlC_2, the most intense peak (104) of Ti_3AlC_2 disappears and the (002) reflection of MXene shifts from 9.7° to 9.1° broadening at the same time. This is consistent with the expected interlayer spacing expansion in passing from Ti_3AlC_2 to Ti_3C_2 MNSs.[30] When the Ti_3C_2 MNSs is further treated in KOH solution, the (002) reflection shifts to 7.1°

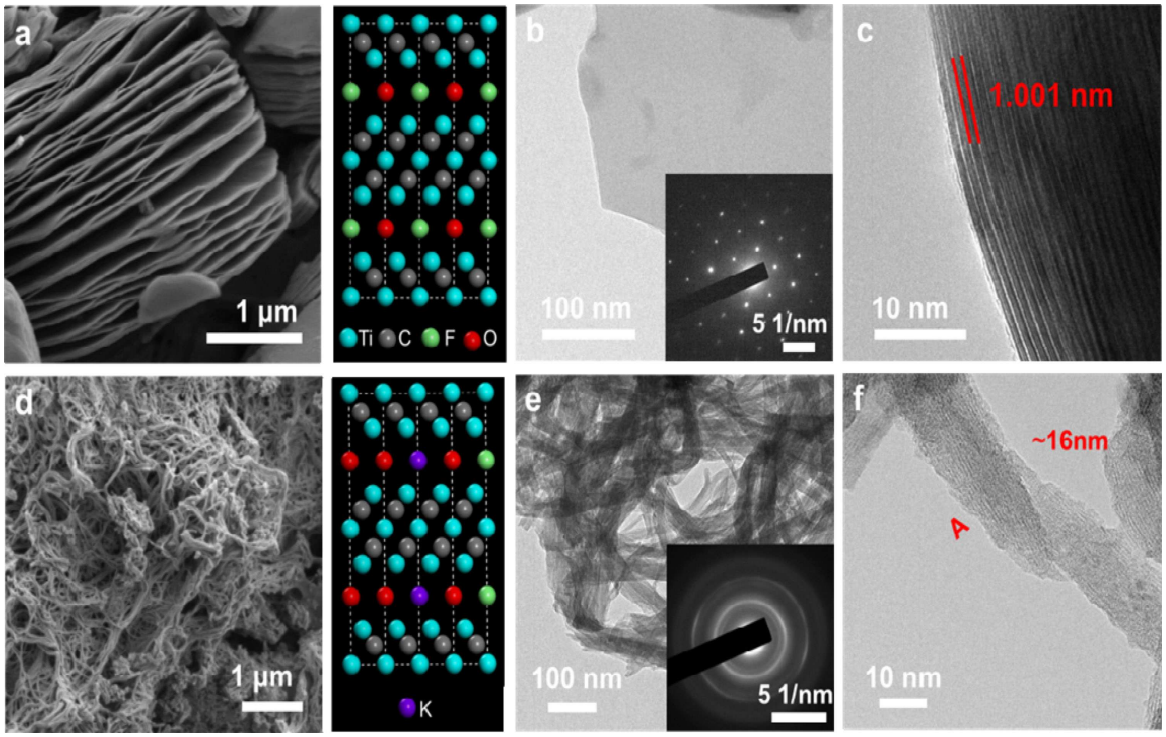

Figure 1. a)SEM image and structural model of Ti_3C_2. MNSs b) Top-view TEM image and electron diffraction pattern of Ti_3C_2 MNSs. c) Cross-sectional TEM image of Ti_3C_2 MNSs. d)SEM image and structural model of Ti_3C_2 MNRs. e) TEM image of Ti_3C_2 MNRs and electron diffraction pattern of Ti_3C_2 MNRs. f) HRTEM image of Ti_3C_2 MNRs, a single MNR with a width of ~16 nm, taken from A position A.

© 2020 Wiley-VCH GmbH

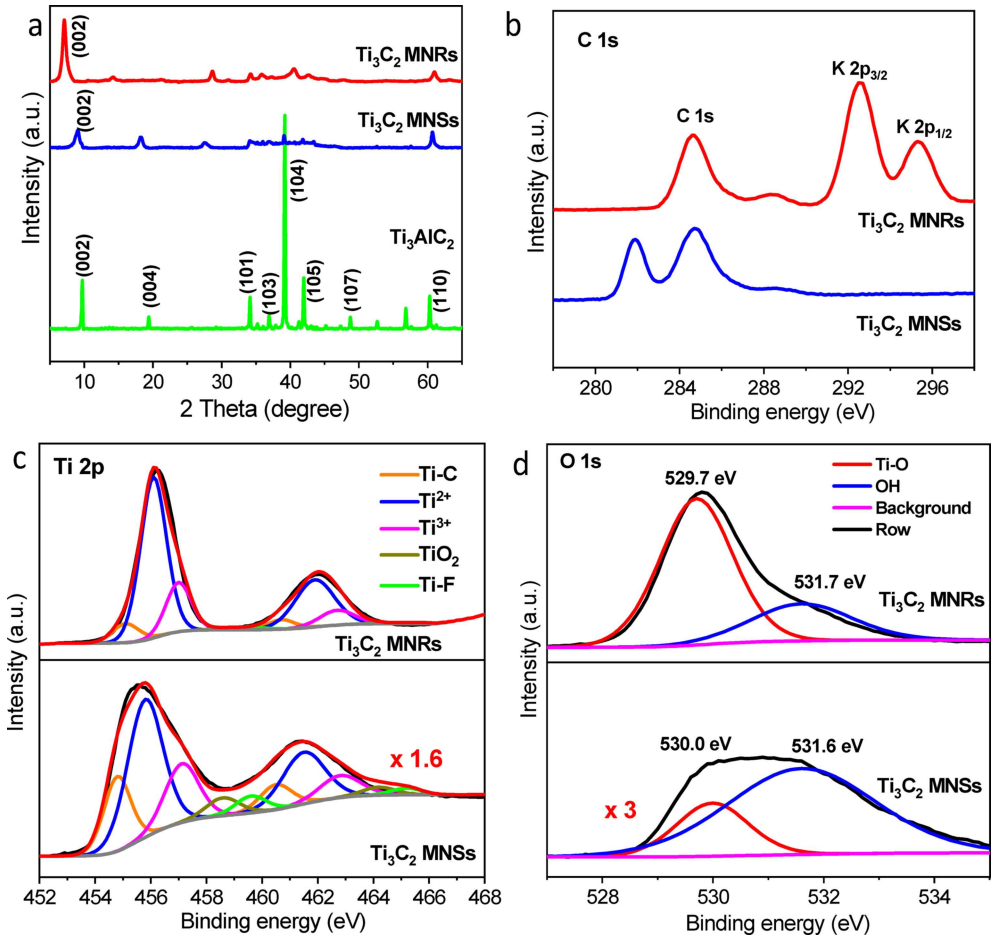

Figure 2. Structural characterization of Ti_3C_2 MNRs, Ti_3C_2 MNSs, and pristine Ti_3AlC_2. a) XRD patterns of Ti_3C_2 MNRs, Ti_3C_2 MNSs, and pristine Ti_3AlC_2. b–d) XPS spectra of Ti_3C_2 MNRs and Ti_3C_2 MNSs in the (b) C 1s, (c) O 1s, and (d) Ti 2p regions.

and further broaden, consistently with the further expansion of interlayer spacing.[23]

The full spectrum X-ray photoelectron spectroscopy (XPS) and associated elemental analysis (Figure S4) confirm the existence of C, K, O and F in Ti_3C_2 MNRs. It also evidenced the large enhancement of the O content which becomes over twice the initial value after the KOH treatment, indicating that the nanoribbon edges are rich in OH groups.

In the C 1s region (Figure 2b), the characteristic peaks of K $2p_{3/2}$ at 292.4 eV and K $2p_{1/2}$ at 295.2 eV are present only in Ti_3C_2 MNRs, but K presence was not detected in Ti_3C_2 MNSs neither in Ti_3AlC_2.This is consistent with XPS elemental analysis (Figure S4b). This accounts for the alkalization of MNRs, consistent with XRD measurement. However, the K atoms do not enter in the Ti_3C_2 MNRs structure to occupy the anion sites, as confirmed by analysis of the lattice spacing of (002) plane in XRD diffractograms.

After the treatment by KOH, the intensity of the XPS Ti–F peaks decreased markedly (Figure S4), while the contents of –OH on the surface increases significantly, indicating that a large amount of –F terminal groups were replaced by hydroxyl groups and consequently the formation of O-terminated Ti_3C_2 MNRs.[31] Energy-dispersive X-ray spectroscopy (EDX) analysis of Ti_3C_2 MNSs and Ti_3C_2 MNR samples confirm this indication (Figure S5). The comparison of the elemental composition by XPS and EDX (SEM) (Figures S4 and S5, respectively) show that after the treatment by KOH, the Ti/C ratio increases owing to the carbon corrosion by KOH. Being XPS detecting the surface composition with a depth less than about 5 nm while the detection depth for SEM is up to about 1 μm, the comparison of Ti/C ratios measured by XPS and EDX indicates a preferential surface carbon removal by the KOH treatment. The EDX of MAX phase (Ti_3AlC_2) and Ti_3C_2 MNSs (Table S1) indicates also that the oxygen content is similar in these two samples.

Figure 2c and d report the XPS Ti 2p and O 1s regions for the Ti_3C_2 MNRs (top) and MNSs (bottom) samples, respectively. Deconvolution of the spectra is also reported according to Lian et al.[23] and Halim et al.[32] For the Ti 2p region, spectra were deconvoluted for Ti–C, Ti^{2+}, Ti^{3+} and TiO_2 components whereas for O 1s region spectra were deconvoluted in Ti–O and –OH components. Figure 2c well indicates that the relative content of TiC decreased after KOH treatment with part of TiC transformed into Ti^{2+} and Ti^{3+}. This result is well consistent with the increase of O content commented before. Ti–F component also

© 2020 Wiley-VCH GmbH

disappears after the MNSs to MNRs conversion. Figure 2d evidences that the conversion leads to a significant increase in the Ti–O component (note that the spectra of Ti_3C_2 MNSs are multiplied by a factor three in intensity).

The electrocatalytic measurements (at room temperature and ambient pressure) were performed in the flow reactor described before operating without a liquid electrolyte in the hemi-cell where the NRR reaction occurs. The flow of highly pure N_2 (further purified by passing through filters to capture eventual presence of NO_x, NH_3 and other possible contaminants) is passed through the electrocatalytic hemi-cell with the ammonia formed being then recovered from the gas outlet stream by absorption in a 1 mM H_2SO_4 solution. The amount of ammonia formed was detected by a spectrophotometric method reported in detail in the Supporting Information. This method is highly sensitive and we consider preferable and more reliable with respect to alternative methods such as NMR, ion-selective electrodes or mass spectrometry. Supporting Information also describes the tests made to exclude the formation of hydrazine (N_2H_4) under our experimental conditions. The protons/electrons for the NRR reactions derive from water electrolysis occurring in the other hemi-cell of the electrocatalytic reactor. A Nafion membrane separates the two hemi-cells (see Figure S1).

A series of control tests were made to verify that ammonia forms from the N_2 present in the flowing gas-phase and not from other N-contaminants (see Figure S3). These tests include monitoring the change in ammonia formation by switching from N_2 to Ar or using labelled nitrogen. By feeding N_2+H_2 at open circuit conditions, it was also verified that the catalytic activity (i.e., not related to electrocatalysis) was negligible. Figure S2 in the Supporting Information reports the experimental protocol for NRR tests used in these experiments, to demonstrate that the detected NH_3 derives from the electrocatalytic reduction of N_2.

Based on cyclic voltammetry (CV) tests (Figure S6), we selected three voltages (in the range from −0.2 to −0.8 V vs RHE) to screen the behaviour of Ti_3C_2 MNRs. Results are reported in Figures S7 and S8. The highest NH_3 yield was obtained at −0.5 V vs RHE. Current density at this voltage is about −1.5 μA and remain stable for at least 3 h of continuous tests. The current density remains stable also in longer term tests (up to about 10 h), showing that the electrocatalyst is stable under these experimental conditions. This result was also in well agreement with CV tests (see Figure S6). At more negative voltage (−0.8 V), the current density instead decreases from the initial −3.5 μA value to about −4.5 μA (after 2 h), indicating thus an in situ transformation during the electrocatalytic tests. At a voltage of −0.2 V, the current density (about −0.5 μA) is instead low, indicating low catalytic activity. Further tests were thus made at −0.5 V. Data reported refer to the behaviour determined after 3 h of continuous tests.

Figure 3 reports the comparison of the rate of ammonia formation per mg of electrocatalysts for the pristine Ti_3AlC_2, Ti_3C_2 MNSs and MNRs samples. Pristine Ti_3AlC_2 and Ti_3C_2 MNSs have a quite comparable low activity in NRR, while Ti_3C_2 MNRs show a more than 5 times higher activity. Faradaic efficiency

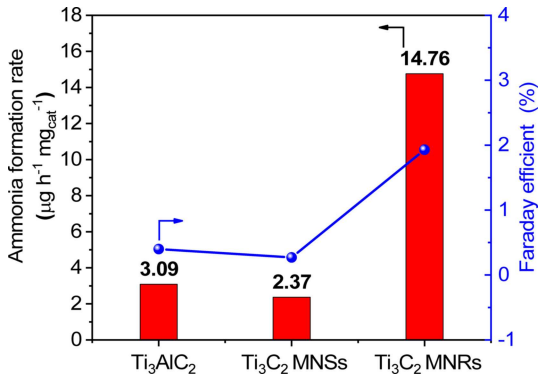

Figure 3. Ammonia formation rate and faradaic efficiency with different electrodes at −0.5 V vs. RHE after 3 h of electrocatalytic tests at room temperature and ambient pressure.

also increases to about 2% after transformation to nanoribbon. A stable current density was shown for all samples, indicating a stable behaviour at the applied voltage at least for 3 h of continuous tests. No significant changes in the sample characteristics were also observed by electron microscopy, XPS and XRD characterization of these materials after the electrocatalytic tests (see Figures S9 and S10). The constant CV data during extended cycles also confirm this stability. These results thus show that morphological, structural, surface and reactivity characteristics of Ti_3C_2 MNRs remain unchanged at least for 10 h of continuous electrocatalytic tests at −0.5 V vs. RHE.

A linear relationship could be observed between the rate of ammonia formation in the three samples reported in Figure 3 and the amount of oxygen on the surface (atomic %) as detected by XPS measurements (Figure 4), suggesting a relationship between these two aspects.

The relationship presented in Figure 4 agrees (among others) with (i) Xia et al.[11] indications that exposed Ti sites (Ti_3C_2OH) are responsible for the improved electron transfer, adsorption and activation of dinitrogen, (ii) theoretical results of

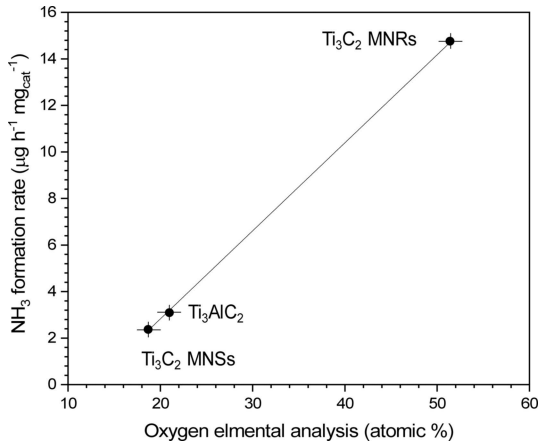

Figure 4. Relationship between ammonia formation rate at −0.5 V vs. RHE and at% of oxygen in the surface as measured by XPS.

© 2020 Wiley-VCH GmbH

Tang et al.[33] that exposed Ti atom close to extra oxygen vacancy are responsible for activity in (defective) MXenes electrocatalysts, (iii) Jin et al.[34] indications that OH-rich MXenes (Ti_3C_2OH) show high NRR performances and (iv) Xia et al.[35] result that surface hydroxyl modification of MXene Ti_3C_2 facilitates the electron transfer and the adsorption and activation of dinitrogen. Therefore, this work shows that the transformation from a 2D-like morphology (nanosheets) to a 3D-like morphology (nanoribbons) leads to a large improvement in the NRR activity, due to an enhanced formation of active sites (likely Ti_3C_2OH) not blocked by F atoms.

To compare these data with literature, Table S2 reports a comparison of reaction conditions, ammonia formation rate and faradaic selectivity of selected state-of-the-art literature results on NRR, organized in four classes of electrocatalytic materials: (a) MXenes, (b) modified and composite electrocatalysts based on MXenes, and electrocatalysts based on (c) noble metals or (d) transition metal oxides/sulphide. The comparison shows that particularly with respect to MXenes electrocatalysts, the electrocatalysts reported here well compares with other published, taking into account of the differences in the operative conditions, and the use here of an electrocatalytic reactor without liquid electrolyte differently from the other cases. Note, in addition, that the scope in this work is not to show record performances, but instead to analyse the role of the conversion from 2D (nanosheet) to 3D-like (nanoribbon) morphology in Ti_3C_2 MXenes.

For a further comparison, some selected results will be compared here. Luo et al.[16] reported for MXene ($Ti_3C_2T_x$) nanosheets a maximum faradaic efficiency of 4.62% and a NH_3 yield rate of 2.7 $\mu g\,h^{-1}\,mg_{CAT}^{<-M>1}$ at a best potential of −0.1 vs. RHE. Xia et al.[11] indicated as best performances (Ti_3C_2 with an increased amount of surface hydroxyl moieties) a yield rate of NH_3 of 1.71 $\mu g\,h^{-1}\,cm^{-2}$ with a faradaic efficiency of about 7%. These performances were in line with those indicated for analogous samples in the reviews by Sun et al.[36] and Li and Wu.[37] We may thus conclude that data reported in Figures 3 and 4 are in line with those earlier reported for Ti_3C_2 nanosheet-type materials, and thus the results reported here evidence a significant enhancement in NRR activity passing from nanosheet to nanoribbon-type morphology. This is related to the formation of OH-rich Ti_3C_2 MXene. This is in agreement with previous literature indications and theoretical studies, but here is for the first time demonstrated the presence of a linear relationship between ammonia formation rate and amount of oxygen on the surface of Ti_3C_2 MXene.

This result evidences that a 2D (nanosheet) morphology is not necessary in MXene materials to show NRR activity, and a different morphology (nanoribbon), not having the same basal planes and type of edges, shows instead an about five times higher NRR activity. Characterization data indicate that in nanoribbon morphology there is a preferential formation of exposed Ti–O sites, which various studies have indicated as responsible for improved electron transfer, adsorption, and activation of N_2.[11,34,35] Present data agree with this interpretation and evidence for the first time the presence of a linear relationship between ammonia formation rate and amount of oxygen on the surface of Ti_3C_2 MXene.

Experimental Section

Synthesis of dlectrocatalysts. To synthesize Ti_3C_2 MXene nanosheets (MNSs), 5 g Ti_3AlC_2 MAX phase was etched by 120 mL 40%HF at 50 °C for 72 h under stirring. Then it was washed and centrifugated by deionized water until pH > 6, followed by vacuum drying at 60 °C overnight. Afterwards. 0.5 g MNSs powder are then treated in 60 mL 6 M KOH for 72 h under Ar atmosphere to avoid the oxidation by oxygen, followed by steps as above.

Electrocatalytic tests. To prepare the electrode, 8 mg of the electrocatalyst was suspended in a 5 mL of ethanol and 50 μL of 10 wt% Nafion solution. The solution was sonicated for 90 min to get a homogeneous mixture which is deposited by spray drying onto a gas-diffusion layer (GDL) which is then hot pressed to a Nafion membrane. The loading amount is 0.2 $mg\,cm^{-2}$ and size of the electrodes was 2 cm^2. All of the electrochemical measurements were carried out at 20 °C using a potentiostat/galvanostat AMEL 2551. A Pt wire was used as the counter electrode. All potentials were measured against Ag/AgCl reference electrode (3 M KCl). A nonconventional type of electrocatalytic cell (operating at atmospheric pressure and room temperature) was developed for these tests, where the solid membrane-electrode assembly separates gas and liquid zones (see Figure S1). The anodic section contains a liquid electrolyte (0.5 M KOH) for water electrolysis to generate the protons and electrons. The reactant N_2 was continuously fed (20 $mL\,min^{-1}$ of N_2 with purity, 99.9999%), and the flow coming out from the electrocatalytic reactor outlet (containing a mixture of N_2 and ammonia) is sent to a liquid absorber containing a 1 mM H_2SO_4 solution. The amount of ammonia formed was detected by spectrophotometry with salicylic acid.

Further details in experimental results and characterizations were described in Supporting Information.

Acknowledgements

This work was made in the frame of the ERC Synergy SCOPE (project 810182), NSFC of China (21972140, 91645117 and 21872144), and PRIN 2017 MULTI-e project nr. 20179337R7, which are gratefully acknowledged. The work was also co-funded through a SINCHEM Grant. SINCHEM is a Joint Doctorate programme selected under the Erasmus Mundus Action 1 Programme (FPA 2013–0037). YL acknowledges the finical supports from LiaoNing Revitalization Talents Program (XLYC1907053) and CAS Youth Innovation Promotion Association (2018220).

Conflict of Interest

The authors declare no conflict of interest.

© 2020 Wiley-VCH GmbH

Keywords: MXenes · metal carbides · N_2 fixation · nanoribbons · nanosheets

[1] J. Li, C. Guo, C. M. Li, *ChemSusChem* **2020**,*13*, 1047.
[2] R. Fang, C. Lu, A. Chen, K. Wang, H. Huang, Y. Gan, C. Liang, J. Zhang, X. Tao, Y. Xia, W. Zhang, *ChemSusChem* **2020**, *13*, 1409.
[3] X. Zhan, C. Si, J. Zhou, Z. Sun, *Nanoscale Horiz.* **2020**, *5*, 235.
[4] J. Pang, R. G. Mendes, A. Bachmatiuk, L. Zhao, H. Q. Ta, T. Gemming, H. Liu, Z. Liu, M. H. Rummeli, *Chem. Soc. Rev.* **2019**, *48*, 72.
[5] T. A. Le, N. Q. Tran, Y. Hong, M. Kim, H. Lee, *ChemSusChem* **2020**, *13*, 945.
[6] J. D. Gouveia, A. Morales-Garcia, F. Vines, F. Illas, J. R. B. Gomes, *Appl. Catal. B* **2020**, *260*, 118191.
[7] Z. Fu, N. Wang, D. Legut, C. Si, Q. Zhang, S. Du, T. C. Germann, J. S. Francisco, R. Zhang, *Chem. Rev.* **2019**, *119*, 11980.
[8] A. Liu, Y. Yang, X. Ren, Q. Zhao, M. Gao, W. Guan, F. Meng, L. Gao, Q. Yang, T. Ma, X. Liang, *ChemSusChem* **2020**, *13*, 3766.
[9] a) S. Wang, B. Li, L. Li, Z. Tian, Q. Zhang, L. Chen, X. C. Zeng, *Nanoscale* **2020**, *12*, 538Y; b) Cheng, J. Dai, Y. Song, Y. Zhang, *Nanoscale* **2019**, *11*, 18132.
[10] J. D. Gouveia, A. Morales-Garcia, F. Vines, J. R. B. Gomes, F. Illas, *ACS Catal.* **2020**, *10*, 5049.
[11] J. Xia, S.-Z. Yang, B. Wang, P. Wu, I. Popovs, H. Li, S. Irle, S. Dai, H. Zhu, *Nano Energy* **2020**, *72*, 104681.
[12] Y. Guo, T. Wang, Q. Yang, X. Li, H. Li, Y. Wang, T. Jiao, Z. Huang, B. Dong, W. Zhang, J. Fan, C. Zhi, *ACS Nano* **2020**, *13*, 8275.
[13] L. Huang, X. Gu, G. Zheng, *Chem* **2019**, *5*, 15.
[14] Y. Gao, Y. Cao, H. Zhuo, X. Sun, Y. Gu, G. Zhuang, S. Deng, X. Zhong, Z. Wei, X. Li, J.-g. Wang, *Catal. Today* **2020**, *339*, 120.
[15] L. R. Johnson, S. Sridhar, L. Zhang, K. D. Fredrickson, A. S. Raman, J. Jang, C. Leach, A. Padmanabhan, C. C. Price, N. C. Frey, A. Raizada, V. Rajaraman, S. A. Saiprasad, X. Tang, A. Vojvodic, *ACS Catal.* **2020**, *10*, 253.
[16] Y. Luo, G.-F. Chen, L. Ding, X. Chen, L.-X. Ding, H. Wang, *Joule* **2019**, *3*, 279.
[17] J. Zhao, L. Zhang, X.-Y. Xie, X. Li, Y. Ma, Q. Liu, W.-H. Fang, X. Shi, G. Cui, X. Sun, *J. Mater. Chem. A* **2018**, *6*, 24031.
[18] X. Wen, J. Guan, *Nanoscale* **2020**, *12*, 8065.
[19] a) M. Shao, Y. Shao, W. Chen, K. L. Ao, R. Tong, Q. Zhu, I. N. Chan, W. F. Ip, X. Shi, H. Pan, *Phys. Chem. Chem. Phys.* **2018**, *20*, 14504; b) B. Qin, Y. Li, Q. Zhang, G. Yang, H. Liang, F. Peng, *Nano Energy* **2020**, 68, 104374; c) K. Chu, Y. Liu, Y. Li, Y. Gao, Y. Tian, H. Zhang, *Appl. Catal. B* **2020**, *264*, 118525; d) K. Chu, Y. Liu, Y. Li, Y. Gao, Y. Tian, *ACS Appl. Mater. Interfaces* **2020**, *12*, 7081–7090; e) K. Chu, J. Wang, Y. Liu, Q. Li, Y. Guo, *J. Mater. Chem. A* **2020**, *8*, 7117–7124.
[20] C. J. Heard, J. Čejka, M. Opanasenko, P. Nachtigall, G. Centi, S. Perathoner, *Adv. Mater.* **2019**, *31*, 1801712.
[21] G. Centi, S. Perathoner, *Coord. Chem. Rev.* **2011**, *255*, 1480–1498.
[22] Z. Wu, T. Shang, Y. Deng, Y. Tao, Q.-H. Yang, *Adv. Sci.* **2020**, *7*, 1903077.
[23] P. Lian, Y. Dong, Z.-S. Wu, S. Zheng, X. Wang, S. Wang, C. Sun, J. Qin, X. Shi, X. Bao, *Nano Energy* **2017**, *40*, 1.
[24] S. Chen, S. Perathoner, C. Ampelli, C. Mebrahtu, D. Su, G. Centi, *Angew. Chem. Int. Ed.* **2017**, *56*, 2699; *Angew. Chem.* **2017**, *129*, 2743.
[25] S. Chen, S. Perathoner, C. Ampelli, C. Mebrahtu, D. Su, G. Centi, *ACS Sustainable Chem. Eng.* **2017**, *5*, 7393.
[26] a) S. Chen, S. Perathoner, C. Ampelli, H. Wei, S. Abate, B. Zhang, G. Centi, *J. Energy Chem.* **2020**, *49*, 22; b) S. Chen, S. Perathoner, C. Ampelli, H. Wei, S. Abate, B. Zhang, G. Centi, *ChemElectroChem* **2020**, 3028.
[27] M. Alhabeb, K. Maleski, T. S. Mathis, A. Sarycheva, C. B. Hatter, S. Uzun, A. Levitt, Y. Gogotsi, *Angew. Chem. Int. Ed.* **2018**, *57*, 5444; *Angew. Chem.* **2018**, *130*, 5542.
[28] J. B. Li, D. Yan, S. J. Hou, Y. Q. Li, T. Lu, Y. F. Yao, L. K. Pan, *J. Mater. Chem. A* **2018**, *6*, 1234.
[29] M. Ghidiu, M. R. Lukatskaya, M. Q. Zhao, Y. Gogotsi, M. W. Barsoum, *Nature* **2014**, *516*, 78.
[30] O. Mashtalir, M. Naguib, V N. Mochalin, Y. Dall'Agnese, M. Heon, M. W. Barsoum, Y. Gogotsi, *Nat. Commun.* **2013**, *4*, 1716.
[31] J. Li, X. Yuan, C. Lin, Y. Yang, L. Xu, X. Du, J. Xie, J. Lin, J. Sun, *Adv. Energy Mater.* **2017**, *7*, 1602725.
[32] J. Halim, K. M. Cook, M. Naguib, P. Eklund, Y. Gogotsi, J. Rosen, M. W. Barsoum, *Appl. Surf. Sci.* **2016**, *362*, 406.
[33] S. Tang, T. Liu, Q. Dang, X. Zhou, X. Li, T. Yang, Y. Luo, E. Sharman, J. Jiang, *J. Phys. Chem. Lett.* **2020**, *11*, 5051.
[34] Z. Jin, C. Liu, Z. Liu, J. Han, Y. Fang, Y. Han, Y. Niu, Y. Wu, C. Sun, Y. Xu, *Adv. Energy Mater.* **2020**, *10*, 2000797.
[35] J. Xia, S.-Z. Yang, B. Wang, P. Wu, I. Popovs, H. Li, S. Irle, S. Dai, H. Zhu, *Nano Energy* **2020**, *72*, 104681.
[36] J. Sun, W. Kong, Z. Jin, Y. Han, L. Ma, X. Ding, Y. Niu, Y. Xu, *Chinese Chem. Lett.* **2020**, *31*, 953.
[37] Z. Li, Y. Wu, *Small* **2019**, *15*, 1804736.

Manuscript received: July 16, 2020
Revised manuscript received: August 6, 2020
Accepted manuscript online: August 12, 2020
Version of record online: ■■, ■■■

© 2020 Wiley-VCH GmbH

COMMUNICATIONS

Show your beauty: MXenes with two-dimensional (2D) structure have been indicated as promising materials for N_2 electrocatalytic conversion to NH_3. The transformation of Ti_3C_2 MXenes from 2D-like nanosheets to 3D-like nanoribbons could enhance significantly the formation of exposed Ti–OH sites to present a superior NH_3 formation rate.